Acta Cryst. (1979). B35, 2614–2625

Deformation Density in Diformohydrazide and Formamide: Experiment *vs* Theory

BY MIRIAM EISENSTEIN

Department of Structural Chemistry, The Weizmann Institute of Science, Rehovot, Israel

(*Received* 14 *May* 1979; *accepted* 23 *July* 1979)

Abstract

The static deformation density of diformohydrazide, $C_2H_4N_2O_2$, has been derived from the low-temperature X-ray data of Hope & Ottersen [*Acta Cryst.* B34, 3623–3626] by least-squares refinement. The intensities were corrected for scan truncation with an empirically estimated effective scan width. The deformation model imposed a minimum of molecular symmetry plus a nuclear cusp constraint and the H atom internal vibrations have been estimated from spectroscopic data. The deformation density shows the expected valence structure and the O atom lone-pair density is slightly asymmetric, perhaps perturbed by hydrogen-bonding. Comparison of coordinates with those from several high-order spherical-atom refinements indicates that detectable asphericity in the O atom density persists to $S > 1{\cdot}7$ Å^{-1}. SCF wavefunctions for formamide, CH_3NO, have been computed with a double-zeta basis and with an extended basis including polarization functions. The extended basis predicts higher bond peaks, largely at the expense of lone-pair regions. Detailed resemblance of the theoretical deformation density with the experimental map of diformohydrazide supports the reliability of both results and indicates that chemical fragments are closely transferable between similar molecules. A quantitative comparison, based on atomic partitioning of the respective deformation densities, shows similar net atomic charges, in accord with plausible resonance structures, larger differences in atomic dipole and second moments. These disagreements may reflect genuine chemical differences and inaccuracy of the wavefunction in peripheral regions.

Introduction

Experimental charge deformation maps (*e.g.* Coppens, 1977 and references therein) have been published for a variety of molecules and in most cases maps of a particular chemical group in different environments are qualitatively similar. Direct comparison of experiment with theory is seldom possible and in fact it is unusual for a theoretical calculation to be illustrated by deformation density maps. But in the few cases where such comparisons have been published (Harel & Hirshfeld, 1975; Rees & Mitschler, 1976; Hase, Schulte & Schweig, 1977; Irngartinger, Hase, Schulte & Schweig, 1977; Stevens, Rys & Coppens, 1978) approximate agreement has been found. The principal aim of this study is to compare static experimental and theoretical deformation densities for similar molecular fragments at the usual qualitative level and also in more quantitative detail. For this purpose, both experimental and theoretical results should be as accurate as current techniques allow.

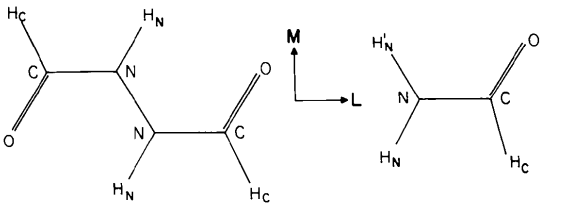

Fig. 1. Diformohydrazide (DFH) and formamide (FA).

A set of 2683 X-ray structure amplitudes, F_o, and their e.s.d.'s, $\sigma(F_o)$, for diformohydrazide (DFH, Fig. 1) at 85 K (Hope & Ottersen, 1978), supplied by the authors, was used to obtain an accurate experimental deformation density of this molecule.

As extended basis-set computations on DFH are too long and cumbersome, formamide (FA, Fig. 1), which is similar to half a molecule of DFH, has been chosen as a model compound for theoretical SCF calculations.

Deformation refinement

Initial model and refinement

The published structure (Ottersen, 1974) of DFH was used as a starting point for a refinement with deformation functions according to the model of Hirshfeld (1977*b*). This model expands the deformation density in a basis of atom-centered functions of the general form

$$\rho_{a,n,k}(\mathbf{r}_a) = N_n r_a^n \exp(-\alpha_a r_a) \cos^n \theta_k. \qquad (1)$$

Use of a deformation model makes it possible to distinguish the asphericity caused by thermal smearing

0567-7408/79/112614-12$01.00

from deformation due to bonding except for H atoms, for which we cannot derive proper thermal parameters from X-ray data alone (Hirshfeld, 1976). We had to adopt a model which could utilize external data and for this purpose the H atom thermal motion was approximated as consisting of a rigid-body molecular motion plus internal C–H and N–H vibrations. The required internal vibration amplitudes were estimated from IR frequencies of formamide (Suzuki, 1960; Itoh & Shimanouchi, 1972). Accordingly, the mean-square stretching and in-plane bending amplitudes were fixed at 0·005 and 0·015 Å^2 respectively for H_N and 0·0057 and 0·0115 Å^2 respectively for H_C. The low-frequency out-of-plane bending vibrations likely to be perturbed by crystal forces were assigned adjustable amplitudes which were refined together with the other parameters. The positional parameters of each H atom were referred to a local polar coordinate system and the C–H and N–H lengths fixed at 1·08 and 0·98 Å respectively before riding correction. Only the angular coordinates of the H atoms were refined.

The molecule is nearly planar and we initially assumed local mirror symmetry for the deformation density of each of the heavier atoms (C, N, O). The cusp functions [$n = 0$ in (1)] on these atoms were omitted in the early stages. For H atoms axial symmetry was assumed and their $n = 4$ functions were given zero coefficients so as to reduce the number of parameters. The approximation for the H atom vibrational behavior causes uncertainty in the deformation density around these atoms and increasing the number of parameters describing this density could only hamper convergence. To account partially for the isotropic contraction of the H atoms due to bonding, their form factor was initially expanded in S ($= 2 \sin\theta/\lambda$) by 20% as if the atomic charge, ζ_H, were 1·2 (Hirshfeld, 1977*b*).

A preliminary rigid-molecule refinement was necessary to estimate the molecular RBM parameters for use in the description of the H atom vibrations. When only C, N, O were considered as forming a rigid body the constrained refinement gave a non-physical description of the motion. Therefore the H atoms were added to the rigid body but with the additional internal motion estimated from IR frequencies of formamide (see above). The refinement converged to provide initial values of the molecular translation and libration amplitudes. These RBM parameters were iteratively adjusted in the same manner as the refinement proceeded.

The refinement sought to minimize the quantity

$$\Delta = \sum w(F_o^2 - k^2 F_c^2)^2,$$

with $w = 1/4F^2\sigma^2(F)$. Analysis of average values of $F_o - kF_c$ *vs* F_o showed that an isotropic extinction correction was necessary. The input values of F_o were accordingly corrected to $F_{corr} = F_o/(1 - c^2 F_o^2)$ with $c =$ 0·00776. Analysis of $w(F_o^2 - kF_c^2)^2$ *vs* F_o showed that the initial error estimates $\sigma(F_o)$ ought to be increased by a term proportional to F. The estimated variance of the strongest reflections was increased further because of the uncertainty in the extinction correction; thus the corrected variance of F had the form

$$\sigma^2_{corr}(F) = \sigma^2(F_o) + (0{\cdot}00256F)^2 + (0{\cdot}0271F)^6,$$

where the extinction-corrected values of F were inserted.

Truncation correction

Another correction had to be introduced because the data we received had not been corrected for scan truncation at high angles. Thus the data showed a systematic sharp drop of $\langle F_o/kF_c\rangle$ for high 2θ values (Fig. 2), similar to the theoretical drop presented by Denne (1977; Fig. 4*b*). The small hump in $\langle F_o/kF_c\rangle$ for $80 < 2\theta < 130°$ is caused by the least-squares refinement which tries to fit the high-order reflections by reducing F_c. This can be done by overestimating the vibration amplitudes and a residual density map plotted with Fourier coefficients $F_o/k - F_c$ at this stage showed a systematic pattern which could be attributed to uniformly large thermal parameters.

The truncation error (Denne, 1977) depends on the width of the experimental $\theta/2\theta$ scan. This width was equal to the $K\alpha_1$, $K\alpha_2$ separation plus 0·9° in 2θ on each side of the scan (Hope & Ottersen, 1978). It was decided to check whether the calculated correction for the actual scan employed was appropriate for the measured data. Such a check seemed desirable because the effective scan width might be modified by factors like monochromatization, wavelength dependence of reflecting power and missetting of the crystal. Hope & Ottersen (1978) indeed found that their truncation correction, based on the actual scan width, may have been insufficient. Accordingly an additional refinement was undertaken in which reflections at $S > 2{\cdot}48$ Å^{-1}

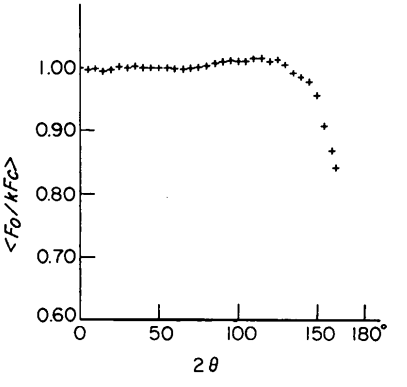

Fig. 2. $\langle F_o/kF_c\rangle$, averaged in overlapping 10° intervals, *vs* 2θ showing the truncation error at high Bragg angles.

were omitted. According to the theoretical plot (Denne, 1977), in a low-order refinement (reflections up to $2\theta \simeq 125°$) the truncation would cause only a small bias which would be absorbed by an isotropic increase in the thermal parameters, together with a small decrease in the scale factor. Therefore we may write:

$$\langle F_o/k' F_c\rangle \simeq \sqrt{T}\exp(AS^2),$$

where T is the theoretical truncation factor in the measured intensities; k' is the apparent scale factor and $\exp(AS^2)$ arises from the isotropic bias in the thermal motion. The angular brackets denote averaging over small intervals in S. For the correct truncation factor T we expect the plot of $\log\langle F_o/k' F_c\rangle - \log\sqrt{T}$ *vs* S^2 to be a straight line. T was computed for different effective scan widths and two of the plots are presented in Fig. 3. The points calculated for the actual scan (0·9° addition in 2θ at each end) did not fit a straight line but such a line could be drawn for the points when a narrower scan (±0·6° in 2θ) was assumed. The slope of this line corresponded to $A = 0{\cdot}0051$ Å^2 which meant that a refinement with corrected data would decrease the temperature parameters, U^{ii}, isotropically by $A/2\pi^2 = 0{\cdot}00026$ Å^2. From the intercept we estimated that the scale factor would increase by 0·4%. In the light of these results the input values of F_o were adjusted according to the empirically determined effective scan width, corresponding to 0·6° in 2θ on each side of the $K\alpha_1$–α_2 doublet. The weights were also reduced in proportion to the correction in F to allow for the uncertainty in the correction in the same way as for the extinction correction described above.

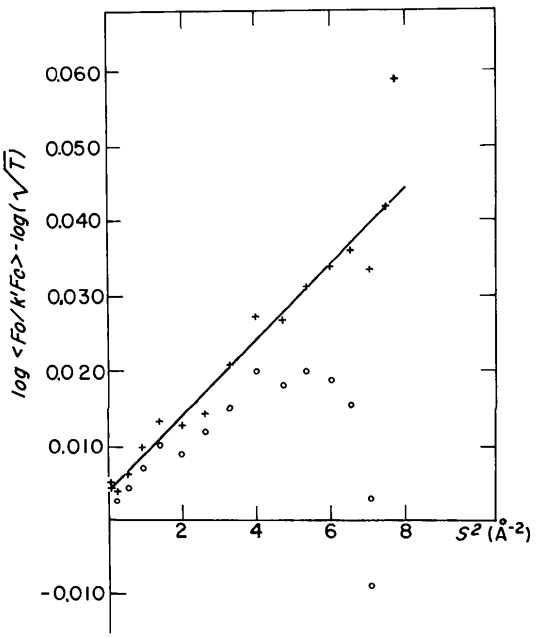

Fig. 3. $\log\langle F_o/k' F_c\rangle - \log\sqrt{T}$ *vs* S^2. T is the calculated truncation factor assuming 2θ scan equal to $K\alpha_1$–α_2 separation plus 0·9° (circles) or 0·6° (crosses) on each side.

Table 1. *Thermal parameters* (Å^2 $\times 10^{-5}$) *from deformation refinements with uncorrected intensity data limited to* $S < 2{\cdot}48$ Å^{-1} (I) *and intensities corrected for scan truncation* (II)

Atom		U_{11}	U_{22}	U_{33}	U_{12}	U_{13}	U_{23}
C	I	881 (4)	708 (4)	701 (4)	−1 (3)	68 (3)	−82 (3)
	II	854 (4)	682 (3)	675 (4)	1 (3)	57 (3)	−82 (3)
N	I	848 (3)	716 (3)	602 (3)	66 (3)	0 (3)	−39 (3)
	II	823 (3)	692 (3)	574 (3)	69 (3)	−12 (3)	−38 (3)
O	I	1090 (4)	898 (4)	694 (3)	−40 (3)	−107 (3)	−78 (3)
	II	1066 (4)	877 (4)	667 (3)	−38 (3)	−119 (3)	−76 (3)

Refinement with the corrected data gave good agreement between $\langle F_o\rangle$ and $\langle kF_c\rangle$, for all S ranges. The thermal parameters became smaller, confirming the conclusion drawn from the earlier residual density map. The change was isotropic and fitted quantitatively the drop estimated from Fig. 3, as can be seen in Table 1. The scale factor increased, about as expected, by a factor 1·003.

The discrepancy factors at the end of this refinement were:

$$R(F) = \sum |F_o - k|F_c||/\sum F_o = 0{\cdot}01582,$$

$$R_w(F^2) = [\sum w(F_o^2 - k^2 F_c^2)^2/\sum wF_o^4]^{1/2} = 0{\cdot}03159,$$

and the goodness of fit

$$G = [\sum w(F_o^2 - k^2 F_c^2)^2/(n-p)]^{1/2} = 1{\cdot}182.$$

These values are lower than the values obtained before the truncation correction: $R = 0{\cdot}01796$, $R_w = 0{\cdot}03519$ and $G = 1{\cdot}816$. Such a drop in R_w is highly significant because in both refinements the same 114 parameters have been refined: 79 deformation parameters; 27 positional and thermal parameters for C, N, O and six positional and thermal parameters for the H atoms; one scale factor and an isotropic extinction coefficient.

Cusp constraint

Refinement of the cusp deformation coefficients [$n = 0$ functions in (1)] added three more parameters and R_w dropped to 0·03157, insignificant according to Hamilton's test (Hamilton, 1965). In this refinement the exponents α_a in (1) were common to all the functions $\rho_{a,n,k}$, centered on a given atom a. We tried an alternative description in which the exponents for the $n = 0$ functions were deduced from the theoretical cusp condition. This condition states (Bingel, 1963) that the electron density $\rho(\mathbf{r})$ at the atomic nucleus ($r = 0$) satisfies

$$\langle \mathrm{grad}\,(\rho)\rangle = -2Z\rho(0)/a_0, \qquad (2)$$

where Z is the nuclear charge and $a_0 = 0{\cdot}5292$ Å is the Bohr radius. The angular brackets denote a spherical average. We applied the appropriate constraint to the

deformation density as follows: the atomic deformation density, $\delta\rho_a$ of atom a in

$$\rho^{\text{mol}} = \sum_a (\rho_a^{\text{spherical atom}} + \delta\rho_a)$$

is expanded as

$$\delta\rho_a(\mathbf{r}_a) = \sum_{n,k} C_{a,n,k}\, \rho_{a,n,k}(\mathbf{r}_a),$$

where the sum is over all deformation functions $\rho_{a,n,k}$ centered on nucleus a. Applying (2) to the density at nucleus a in the molecule, assuming negligible contributions from deformation functions centered on neighboring nuclei, we have:

$$\langle \text{grad}\,(\rho_a^{\text{spherical atom}})\rangle + \langle \text{grad}\,(\delta\rho_a)\rangle = -2Z_a(\rho_a^{\text{spherical atom}} + \delta\rho_a)/a_0.$$

Subtraction of the corresponding equation for the isolated atom leaves us with the cusp condition for the atomic deformation:

$$\langle \text{grad}\,(\delta\rho_a)\rangle = -2Z_a(\delta\rho_a)/a_0.$$

The only function contributing to $\delta\rho_a$ at the nucleus or to its spherically averaged gradient is the cusp function $\rho_0 = N_0 \exp(-\alpha_a r_a)$. Thus we have for this term

$$\alpha_{a,0} = 2Z_a/a_0.$$

Substitution of these $\alpha_{a,0}$ values for the $n = 0$ term on all atoms and refinement of their coefficients reduced R_w to 0·03146. In this refinement we used the uncontracted H atom form factor with $\zeta_H = 1{\cdot}0$.

Final refinement

The next step was to check the mirror symmetry which had been imposed on the deformations of the heavier atoms (see above). We saw no reason to relax this restriction except for the O atom, which accepts a hydrogen bond from a neighboring molecule at an angle of 19·7° above the mean molecular plane. Removal of the mirror symmetry constraint for the O atom added 13 more deformation coefficients and R_w dropped to 0·03119. The final results were obtained after an additional refinement of the rigid-body parameters used in describing the H atom thermal motion. The agreement factors were: R = 0·01562, R_w = 0·03118 and the goodness of fit G = 1·17. The value of R can be compared to R = 0·0268 obtained by Hope & Ottersen (1978), showing that the deformation refinement gives a much better fit to the experimental data. A residual density map, $\Delta\rho = \sum (F_o/k - F_c)\cos[-2\pi(hx + ky + lz)]$, computed at this stage showed no special features, confirming that the experimental intensities were adequately accounted for by the model. A reasonable check on the validity of the thermal parameters is the rigid-bond test (Hirshfeld, 1976). The agreement of the amplitudes of motion along the bonds for bonded atoms (Table 2) is excellent in view of the e.s.d.'s of the heavy-atom vibration parameters U^{ij}, which average 4×10^{-5} Å^2 (Table 4).

Table 2. *Mean-square amplitudes* (Å^2 $\times 10^{-5}$) *of motion along bonds from the final deformation refinement* (*Def.*) *and from high-order* ($S > 1{\cdot}6$ Å^{-1}) *spherical-atom refinement* (*HO*)

Bond		Atom 1	Atom 2
C–N	Def.	559	551
	HO	581	550
C=O	Def.	618	616
	HO	641	604

Comparison with high-order refinements

The positional and thermal parameters for C, N, O were also compared to values obtained from a high-order spherical-atom refinement. Such refinements had been performed by Hope & Ottersen (1978, 1979) but it seemed desirable to check whether the results would be sensitive to the differences in truncation correction and in the weights. The H atom parameters were taken from the deformation refinement and fixed, while 27 positional and thermal parameters for C, N, O and the scale factor were refined against 1966 reflections with $S > 1{\cdot}6$ Å^{-1}. This refinement led to R = 0·02141, R_w = 0·04782 and G = 1·210 for the high-angle data. The parameters from the deformation and the high-order refinements are compared in Tables 3 and 4. The agreement in positional coordinates (Table 3) is good, with only the O atom showing an appreciable discrepancy. The nature of this discrepancy is examined in Table 5, where the atomic positions from the two refinements and from two refinements performed by Hope & Ottersen (1978) are compared in a molecular coordi-

Table 3. *Fractional atomic coordinates from the final deformation refinement* (*Def.*) *and from the high-order* ($S > 1{\cdot}6$ Å^{-1}) *spherical-atom refinement* (*HO*)

Atom		x	y	z
C	Def.	0·10707 (5)	0·21814 (3)	0·13867 (3)
	HO	0·10703 (5)	0·21813 (2)	0·13869 (2)
N	Def.	−0·06489 (4)	0·10462 (3)	0·00328 (2)
	HO	−0·06492 (4)	0·10464 (2)	0·00325 (1)
O	Def.	0·38015 (8)	0·14620 (4)	0·26201 (3)
	HO	0·38055 (5)	0·14608 (2)	0·26211 (2)
H_C	Def.	−0·01613	0·37992	0·12978
H_N	Def.	−0·27712	0·16732	−0·09309

nate system (Fig. 1). Three conclusions emerge from this comparison: (*a*) The C and N atom positions from all four refinements agree within 0·0003 Å. (*b*) The spread in O atom positions reaches 0·0015 Å and extends approximately along the direction of the C=O bond. (*c*) As S_{min} for the high-order refinements is increased, the O atom converges slowly towards the position from the deformation refinement. This suggests that the spherical-atom model biases the apparent O atom position towards its lone-pair density and this bias persists even in data above 1·7 Å^{-1}.

Comparison of the thermal parameters from our high-order and deformation refinements (Table 4) shows excellent agreement for N, almost as good for O, and a small systematic discrepancy for C, whose amplitudes are higher in the high-order refinement. The excess relative motion of the C atom is revealed by the rigid-bond test for the high-order refinement (Table 2). This test supports the superiority of the deformation model over use of high-order data with the spherical-atom model for discriminating between bonding effects and vibrational smearing. Comparing our results to those obtained by Hope & Ottersen (1978), we see that our temperature factors are almost isotropically smaller for all atoms, probably because of the larger magnitude of our truncation correction.

Table 4. *Thermal parameters* (Å^2 ×10^{-5}) *from the final deformation refinement* (*Def.*) *and from the high-order* ($S > 1{\cdot}6$ Å^{-1}) *spherical-atom refinement* (*HO*)

Atom		U_{11}	U_{22}	U_{33}	U_{12}	U_{13}	U_{23}
C	Def.	841 (5)	668 (4)	661 (4)	2 (3)	50 (3)	−82 (3)
	HO	863 (4)	689 (4)	678 (4)	−3 (3)	62 (3)	−79 (3)
N	Def.	831 (4)	698 (4)	581 (3)	71 (2)	−13 (2)	−38 (2)
	HO	836 (4)	690 (3)	581 (3)	74 (2)	−8 (2)	−38 (2)
O	Def.	1086 (6)	890 (5)	673 (4)	−33 (3)	−112 (3)	−76 (3)
	HO	1068 (4)	891 (4)	668 (3)	−33 (2)	−118 (2)	−70 (2)
H_C	Def.	2396	1420	2042	334	470	−128
H_N	Def.	1750	2045	1505	336	−17	354

Table 5. *Cartesian coordinates* (*see Fig.* 1 *for molecular axes*) *and bond lengths* (Å) *from three high-order spherical-atom refinements and from the deformation refinement* (*Def.*)

Results for $S > 1{\cdot}5$ and $S > 1{\cdot}7$ Å^{-1} are from Hope & Ottersen (1978).

Atom		*L*	*M*	*N*
C	$S > 1{\cdot}5$	1·66975	−0·60108	0·00112
	$S > 1{\cdot}6$	1·66969	−0·60087	0·00098
	$S > 1{\cdot}7$	1·66968	−0·60100	0·00104
	Def.	1·66960	−0·60090	0·00123
N	$S > 1{\cdot}5$	0·33856	−0·60113	−0·00160
	$S > 1{\cdot}6$	0·33846	−0·60110	−0·00157
	$S > 1{\cdot}7$	0·33850	−0·60109	−0·00142
	Def.	0·33860	−0·60090	−0·00169
O	$S > 1{\cdot}5$	2·35430	0·43105	−0·00018
	$S > 1{\cdot}6$	2·35430	0·43104	−0·00021
	$S > 1{\cdot}7$	2·35417	0·43072	−0·00020
	Def.	2·35388	0·42962	−0·00063

C–N	$S > 1{\cdot}5$	1·3312	C–O	$S > 1{\cdot}5$	1·2385
	$S > 1{\cdot}6$	1·3312		$S > 1{\cdot}6$	1·2384
	$S > 1{\cdot}7$	1·3312		$S > 1{\cdot}7$	1·2381
	Def.	1·3310		Def.	1·2370

Experimental maps

Two types of experimental deformation maps have been obtained: static deformation density maps evaluated from the deformation parameters (Figs. 4*a*, 5, 6*a*) and dynamic deformation densities obtained by Fourier difference synthesis with high-order positional and thermal parameters (Figs. 6*b*, 7). The latter were

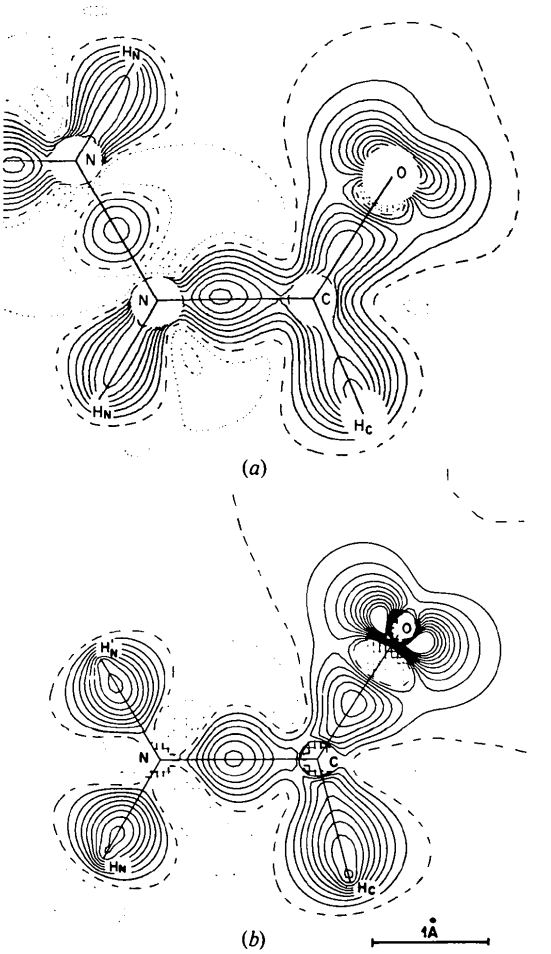

Fig. 4. Deformation density in mean molecular plane. Contour interval 0·1 e Å^{-3}; zero contour dashed; negative contours dotted. (*a*) DFH: experimental map; blank regions around atomic nuclei have e.s.d. $\sigma(\delta\rho) > 0{\cdot}1$ e Å^{-3}. (*b*) FA: edz map.

calculated at a resolution given by $S_{max} = 1{\cdot}7$ Å^{-1}. Our dynamic deformation maps are very similar to those obtained by Hope & Ottersen (1979) except that the density peaks are higher. This is probably related to the smaller thermal parameters in our refinement (see above).

To make possible a comparison of experimental and theoretical static deformation maps, it was necessary to define the experimental density of a single molecule of DFH, *i.e.* to define a molecule within a crystal. Hirshfeld (1977*a*) has defined an atomic fragment within a molecule. The same recipe can be used to define the atoms in a crystal; these can then be summed to yield the density of a molecule. Because the crystal is infinite it becomes necessary to operate on a finite region surrounding our chosen molecule. We chose a half-molecule comprising one asymmetric unit as the center of our microcrystal. For each atom in the neighboring asymmetric units, we calculated the shortest distance to any atom of the central half-molecule. Atoms making no contact <4·7 Å were rejected. The value of 4·7 Å was chosen because with this limit all atoms in the asymmetric units involved in hydrogen bonds with the central unit were included. This left a small microcrystal, comprising 86 atoms, whose charge density was evaluated by direct summation and partitioned into atomic fragments according to the method of Hirshfeld (1977*a*). In a second computation the limiting approach radius was increased to 8 Å. The new microcrystal contained 311 atoms but the atomic fragments of the central half-molecule did not change significantly. These were taken to represent the atomic fragments in the crystal.

Now we could define the molecular density as the sum of the atomic fragments comprising one whole molecule. Fig. 4(*a*) shows the molecular deformation density so defined, in the best plane defined by the heavy atoms. Sections perpendicular to this mean molecular plane are shown in Fig. 5. While the e.s.d. $\sigma(\delta\rho)$ (Rees, 1977) is quite small at bonding peaks and in lone-pair regions (Table 6) it is very high, as expected, at the atomic centers and is certainly still underestimated in these regions. The blank spaces around the atomic centers in Figs. 4(*a*), 5, 6(*a*) are regions where $\sigma(\delta\rho) > 0{\cdot}1$ e Å^{-3}.

The maps clearly show maxima in the bonding regions and in the O and N atom lone-pair regions. The O atom lone-pair lobes are only slightly perturbed by

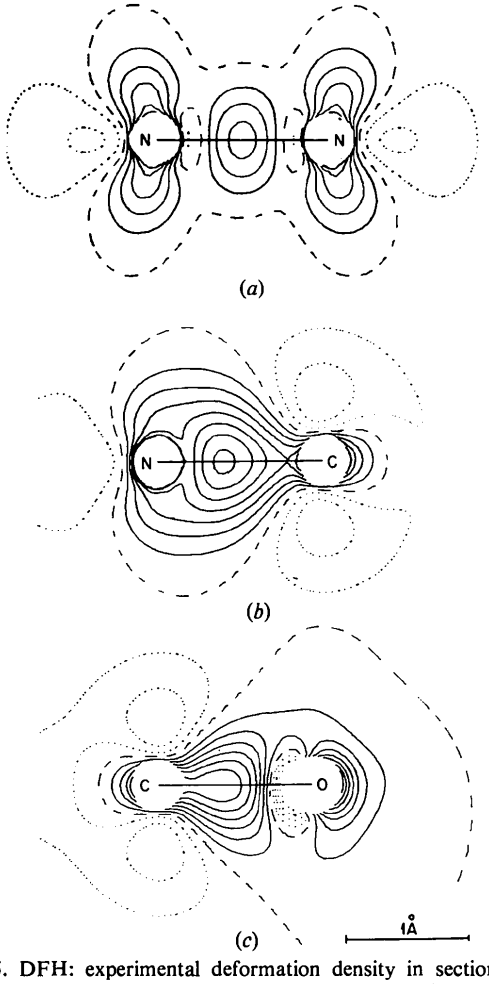

Fig. 5. DFH: experimental deformation density in sections perpendicular to the mean molecular plane through (*a*) N–N; (*b*) N–C; (*c*) C=O. Contours as in Fig. 4.

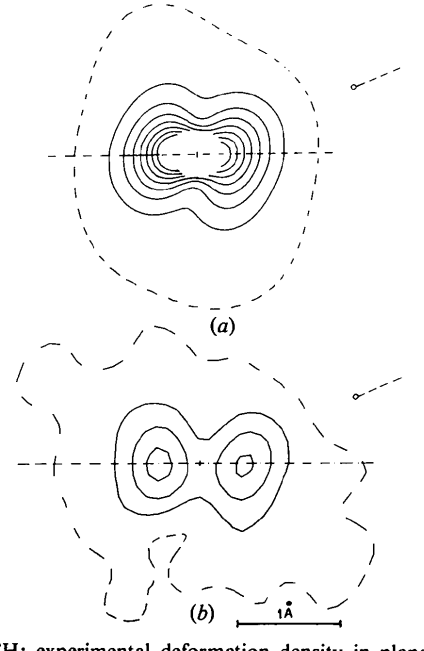

Fig. 6. DFH: experimental deformation density in plane perpendicular to C=O bond passing 0·1 Å behind the O atom. Mean molecular plane horizontal. Dashed line marks projection of N–H bond of neighboring molecule. Contours as in Fig. 4. (*a*) Static density from deformation refinement. (*b*) Dynamic density from *X*–*X* (high-order) difference synthesis.

Table 6. *DFH: Deformation densities and e.s.d.'s* (e $Å^{-3}$) *at bond maxima and atomic centers*

	$\delta\rho$	$\sigma(\delta\rho)$
N–N	0·345	0·024
N–C	0·735	0·022
C–O	0·683	0·030
C	19	8
N	58	16
O	95	41
H_N	0·45	0·16
H_C	0·76	0·31

the hydrogen bond. This perturbation is observed mainly in the zero contour and it seems that there is less density in the lone-pair lobe that is directed towards the H atom. A similar picture was observed in the deformation densities of other carbonyl compounds in which one of the carbonyl lone-pair lobes accepts a hydrogen bond, *e.g.* the deformation density of the $HC_2O_4^-$ ion in $(CH_3)_2NH_2HC_2O_4$ (Thomas, 1977) and in $NaHC_2O_4.H_2O$ (Tellgren, Thomas & Olovsson, 1977) and the theoretical deformation density of formic acid cyclic dimer obtained from a double-zeta wavefunction (Eisenstein, 1978).

The deformation density has a steep gradient at the O atom nucleus, which probably accounts for the persistence of the asphericity shift of this atom in the high-order refinements (Table 5). A similar gradient is found in the SCF deformation density of formamide (Fig. 4*b*) and so is probably genuine.

The structure of the molecule suggests sp^2 hybridization for C, N, O and this is confirmed in the perpendicular sections (Fig. 5). Section 5(*c*) shows the elongation of the C=O bond peak in the perpendicular plane due to π bonding. The N atom can either keep two of its valence electrons in a lone-pair $p\pi$ orbital as in (I) or participate in a π bond with the C atom to form the charge-separated resonance structure (II). Sections 5(*a*) and 5(*b*) show appreciable localization of the π density on the N atom together with a significant elongation of the N–C bond peak in the π plane. We conclude that the DFH electronic structure may be described by three main resonance contributions (I), (II) and (II′):

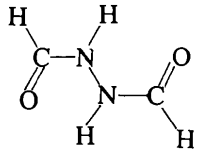

(I)

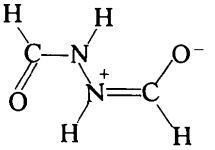

(II)

where (II′) is related to (II) by inversion in the molecular center of symmetry.

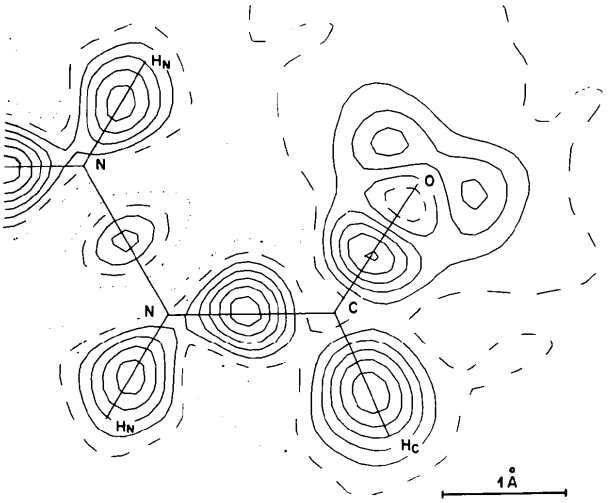

Fig. 7. DFH: dynamic deformation density in mean molecular plane from *X–X* (high-order) difference synthesis. Contours as in Fig. 4.

Stevens, Rys & Coppens (1978) found the O atom lone-pair peaks in formamide above and below the mean molecular plane. The static deformation density in DFH in a section perpendicular to the C=O bond axis 0·1 Å behind the O atom nucleus is shown in Fig. 6(*a*) together with the dynamic *X–X* (high-order) density in the same plane (Fig. 6*b*). Both show slight asymmetry relative to the molecular plane but the peaks are clearly in the plane.

It is interesting to compare the dynamic *X–X* (high-order) deformation density of DFH (Fig. 7) with the vibrationally smeared theoretical density of formamide (Stevens, Rys & Coppens, 1978). The positions and shapes of the deformation density peaks and even their heights are very similar. No quantitative comparison between these maps is possible because the thermal motions are different; the experimental vibration parameters for FA are twice as large as those for DFH, although the anisotropy is very similar in the two molecules.

Theoretical computations

Ab initio–LCAO–GTO–SCF computations were performed on formamide (FA) with the *POLYATOM* set of programs (Metzgar & Bloor, 1973). We started with a double-zeta (dz) computation with 36 contracted basis functions, using the [4*s*,2*p*] contracted basis set of Dunning (1970) based on Huzinaga's (1965) 10*s* 6*p* atomic basis or, for H atoms, the [2*s*] set scaled to $\zeta_s = 1{\cdot}2\ a_0^{-1}$. The molecular geometry was taken from Kurland & Wilson (1957). Next, an extended-basis (edz) computation was undertaken in which the dz basis was augmented by two sets of *d* functions

centered on each of the heavier atoms C, N, O and two sets of p functions on each H atom. The additional functions consisted of one Gaussian with an exponent of 1·5 and a second with 0·5 a_0^{-2}. The number of contracted basis functions was 90 and the same geometry as for the dz computation was used. The resultant energies appear in Table 7. The edz energy is lower than the dz energy by 0·0955 a.u. (250·6 kJ mol^{-1}) and is comparable to the energy obtained in other extended-basis computations (Stenkamp & Davidson, 1977 and references therein; Stevens, Rys & Coppens, 1978).

Theoretical deformation maps

In order to derive theoretical deformation densities, spherically averaged atomic electron distributions calculated with the same dz basis were subtracted, except that the H atom basis was not scaled.

Contour maps of the dz and edz deformation densities, and of their difference $\rho_{edz} - \rho_{dz}$, are plotted in Figs. 4(*b*), 8, 9 and 10. Comparison of the theoretical calculations (Figs. 8*b*, 10) shows that inclusion of polarization functions leads to a migration of electronic charge into the bonds from behind the atoms and especially from the lone-pair regions of the N and O atoms.

As in DFH, sp^2 hybridization is expected for C, N and O. Thus, two resonance structures describe the electronic structure of FA:

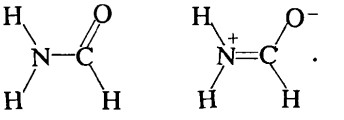

(I) (II)

The N–C and C–O bond peaks show the expected elongation in the out-of-plane direction (Fig. 9) but the shapes of the lone-pair peaks, concentrated in the molecular plane for the O and in the perpendicular plane for the N atom, show that the non-polar structure (I) is predominant.

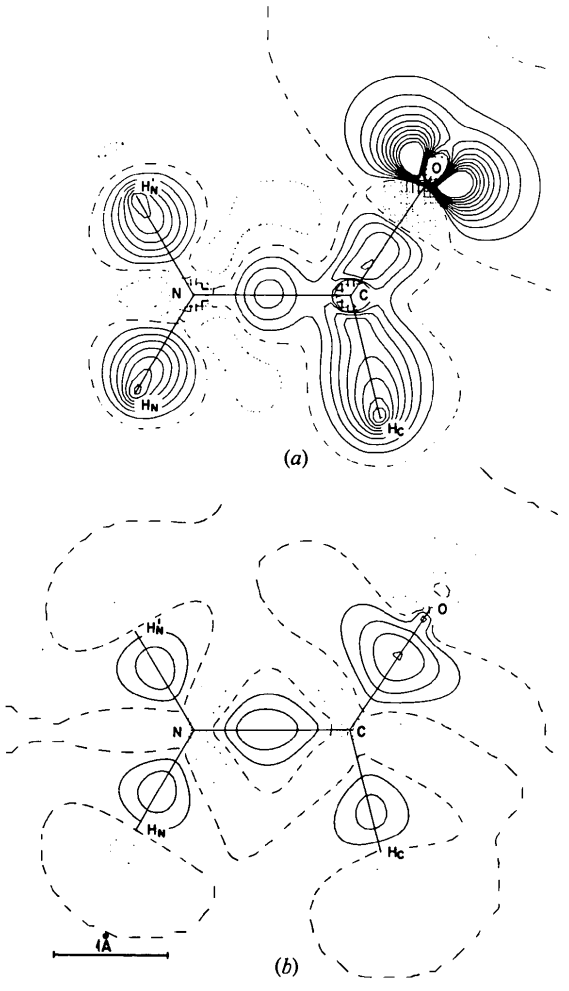

Fig. 8. FA: SCF deformation density in molecular plane. Contours as in Fig. 4. (*a*) $\delta\rho_{dz}$. (*b*) $\delta\rho_{edz} - \delta\rho_{dz}$.

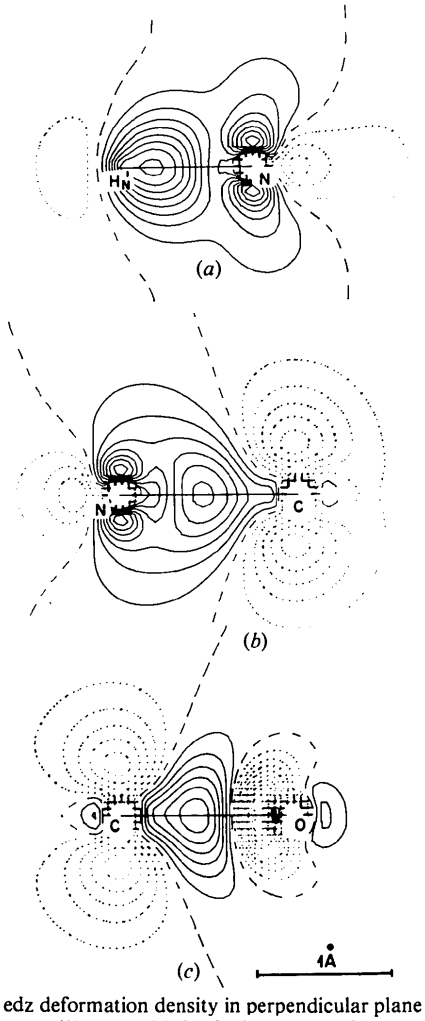

Fig. 9. FA: edz deformation density in perpendicular plane through (*a*) H'_N–N; (*b*) N–C; (*c*) C=O. Contours as in Fig. 4.

Quantitative description of the SCF deformation density

Tables 8 and 9 compare net atomic charges and atomic dipole and second moments for DFH, FA (edz) and FA (dz) as defined by Hirshfeld (1977*a*). The integrations for FA have been performed on a rectangular grid of 0·1 Å. Previous experience has shown such a grid to be adequate and this is supported by the small calculated charge imbalance of −0·002 e.

The dz and edz calculations show essentially the same pattern of atomic charges and moments and this is in overall accord with the postulated resonance structures. As expected, the O atom is negatively charged while the NH_2 group, as a whole, bears a net positive charge. The C atom, bonded to two electronegative ligands, is positive. In general, the polarity of each bond, as measured by the difference in atomic charge at its two ends, follows the relative electronegativities of the bonded atoms.

The atomic dipoles are small and readily interpretable only for the terminally bonded atoms. Thus, the H atom dipoles are all directed along the bond, with the negative end pointing into the bond. The O atom dipole shows the opposite behavior, with its negative end directed away from the bond towards the lone-pair region (Fig. 4*b*). The small dipole on the C atom is close to the C=O bond direction.

Values of the second moment express two kinds of change in the atomic charge distribution: an isotropic part, with the same sign as q, corresponding to the net gain or loss of valence density; and a second part, which may be anisotropic, denoting contraction (positive second moment) or expansion (negative values) of the atomic density. Thus, the C and H atoms have net positive charge and positive second moments, indicating that the loss of charge is from the outer regions of these atoms. In the H atoms the contraction of the remaining charge is nearly isotropic while the C atom has an especially large positive μ_{NN} which implies that it has lost charge primarily from its π orbital, as may be seen in the perpendicular sections (Fig. 9). The O atom has gained charge (negative q), which is distributed fairly isotropically (negative $\mu_{LL} \simeq \mu_{MM} \simeq \mu_{NN}$). In this respect the contour diagrams are perhaps misleading; the deformation density in the σ plane is highly concentrated in the lone-pair peaks (Fig. 4*b*) and so much more conspicuous than the very diffuse excess density in the out-of-plane direction (Fig. 9*c*). The excess charge on the N atom has gone entirely into the π orbital (slightly negative μ_{NN}) while the σ density is strongly concentrated (positive $\mu_{LL} \simeq \mu_{MM}$).

The small differences between the dz and edz results (Tables 8, 9) show that the main influence of the polarization functions is indeed to polarize the charge on the several atoms. The atomic charges q are very slightly reduced in magnitude while the most prominent

Table 7. *SCF energies* (a.u.) *of formamide from double zeta* (*dz*) *and double-zeta-plus-polarization* (*edz*) *basis sets*

	dz	edz
Total energy	−168·880006	−168·975520
Kinetic (T)	168·95703	168·69503
Potential (V_{ne})	−539·91175	−540·08125
Potential (V_{ee})	130·97264	131·30863
Virial $-V/2T$	0·99977	1·00083

Table 8. *Atomic charges* (e) *and dipole moments* (e Å) *for DFH and FA*

		q	μ_L	μ_M	μ_N	μ	$\alpha(°)$*
C	DFH	0·162	−0·020	0·005	0·0	0·021	166
	FA(edz)	0·205	−0·009	−0·040	0·0	0·041	−102
	FA(dz)	0·212	−0·011	−0·019	0·0	0·022	−120
N	DFH	−0·013	−0·051	0·024	−0·001	0·057	155
	FA(edz)	−0·146	−0·011	0·005	0·0	0·012	156
	FA(dz)	−0·151	0·006	−0·002	0·0	0·006	−15
O	DFH	−0·384	−0·004	−0·027	−0·003	0·027	−98
	FA(edz)	−0·382	−0·050	−0·060	0·0	0·078	−130
	FA(dz)	−0·387	−0·110	−0·141	0·0	0·179	−128
H_C	DFH	0·076	0·022	−0·060	0·001	0·064	−70
	FA(edz)	0·053	0·012	−0·076	0·0	0·077	−81
	FA(dz)	0·056	0·009	−0·070	0·0	0·071	−83
H_N	DFH	0·163	−0·025	−0·036	−0·003	0·044	−125
	FA(edz)	0·131	−0·057	−0·092	0·0	0·108	−122
	FA(dz)	0·133	−0·055	−0·090	0·0	0·105	−121
H'_N	FA(edz)	0·136	−0·060	0·090	0·0	0·108	124
	FA(dz)	0·135	−0·060	0·088	0·0	0·106	124

*α gives the direction of the positive end of the atomic dipole measured from the L axis (Fig. 1); positive α denotes rotation towards $+M$ axis.

Table 9. *Second moments* (e Å^2) *of atomic deformation densities in DFH and FA*

		μ_{LL}	μ_{MM}	μ_{NN}	μ_{LM}	μ_{LN}	μ_{MN}
C	DFH	0·167	0·165	0·355	−0·024	−0·009	−0·002
	FA(edz)	0·069	0·080	0·230	−0·044	0·0	0·0
	FA(dz)	0·073	0·097	0·209	−0·037	0·0	0·0
N	DFH	0·124	0·164	0·200	0·010	0·0	−0·001
	FA(edz)	0·080	0·097	−0·004	−0·002	0·0	0·0
	FA(dz)	0·088	0·104	−0·038	−0·002	0·0	0·0
O	DFH	0·056	0·020	0·064	−0·005	0·003	0·004
	FA(edz)	−0·088	−0·064	−0·072	0·028	0·0	0·0
	FA(dz)	−0·099	−0·072	−0·080	0·034	0·0	0·0
H_C	DFH	0·084	0·072	0·084	0·014	−0·003	−0·006
	FA(edz)	0·079	0·073	0·087	0·004	0·0	0·0
	FA(dz)	0·080	0·072	0·085	0·004	0·0	0·0
H_N	DFH	0·084	0·051	0·116	−0·023	0·003	0·005
	FA(edz)	0·098	0·093	0·069	−0·008	0·0	0·0
	FA(dz)	0·099	0·092	0·064	−0·008	0·0	0·0
H'_N	FA(edz)	0·092	0·089	0·069	0·002	0·0	0·0
	FA(dz)	0·092	0·087	0·062	0·001	0·0	0·0

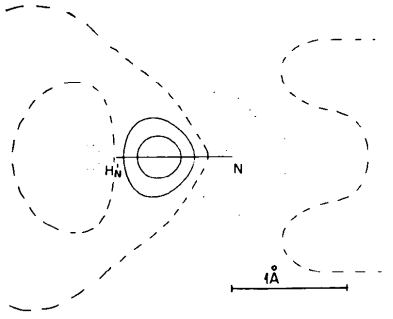

Fig. 10. FA: $\delta\rho_{edz} - \delta\rho_{dz}$ in perpendicular plane through H'_N–N bond. Contours as in Fig. 4.

changes are in the atomic dipoles. These reflect the enhanced polarization of charge into the bonds, Fig. 8(*b*). Thus the dipole moments on the H atoms are slightly increased while the polarization of the O atom away from the bond is sharply reduced. On the C atom the polarization functions serve to increase the magnitude of the atomic dipole and to change its direction, apparently by virtue of the enhanced charge migration preferentially into the C=O and C–N bonds. The second moments show an increased contraction of π density towards the molecular plane (positive $\Delta\mu_{NN}$ on all atoms) together with a moderate reduction in both the in-plane contraction on C and N and the in-plane expansion on O.

Comparison of experimental and theoretical deformation densities

A comparison of the deformation densities in formamide and diformohydrazide will reveal discrepancies arising from four separate sources:

(*a*) genuine chemical differences between the bonding in the two molecules;

(*b*) crystal-induced perturbations of the deformation density in DFH;

(*c*) experimental and model errors in the DFH deformation density;

(*d*) inaccuracy of the FA wavefunction due to errors in the geometry, basis-set limitations and neglect of electron correlation.

Where the two maps differ any or all of these effects may be responsible. Where they agree it is probable, but not certain, that all four are negligible.

Qualitative comparison

Comparison of the static experimental DFH and the edz theoretical FA deformation density maps shows strong resemblance in position, shape and height of most peaks (Fig. 4). We can therefore surmise that, on the whole, the two molecules are closely similar and both the theoretical and the experimental static deformation densities are good approximations to the truth. The most conspicuous differences are in the O atom lone-pair peaks and in the N atom *p* orbitals, which seem to be more compact in the theoretical computation. We do not expect the regions about the atomic centers to be comparable because of the high e.s.d.'s in the experimental results at these regions. The dz maps are much less similar to the experimental maps.

Quantitative comparison

The integrations for DFH have been performed on a rectangular grid of 0·2 Å, except for the cusp regions where the grid was 0·04 Å. The net charge imbalance

for a DFH molecule was 0·009 e. An estimate of the error in the experimental quantities listed in Tables 8 and 9 may be derived from the least-squares covariance matrix (Rees, 1977). This has not been done because the calculations are lengthy and the results are dubious since they do not allow properly for systematic errors, which could be appreciable.

The agreement in atomic charges between DFH and FA (edz) is good provided we compare the nitrogen atomic charge in DFH with the net charge on the $N-H'_N$ group in FA. Both molecules show a pronounced migration of charge from NH or NH_2 to O as required by the resonance structures suggested above.

Comparison of atomic dipole moments shows that the experimental values of μ are systematically smaller than the theoretical values except on the N atom, but here the difference between molecules invalidates any quantitative comparison. For the H atoms there is a reasonable agreement in the direction of the atomic moments, which in both cases are in the direction of the bond within a few degrees. For the O atom there is a discrepancy in both magnitude and direction, which may partly be explained by the influence of hydrogen-bonding in DFH. In FA the dipole moment on the O atom is consistent with approximate *mm* symmetry about the C=O bond. This symmetry is perturbed by the hydrogen bond in the DFH crystal, which causes a change in the direction of the dipole moment indicating a charge migration away from the H atom. This migration is very diffuse and is observed mainly in the zero contour in the deformation maps (see above).

The second-moment diagonal components (Table 8) are larger for the experimental results and positive, implying a contraction of all atoms in DFH. The contraction of the H atoms is fairly isotropic and more or less the same in DFH and FA (edz). For the C atoms the contraction is much larger in DFH but both molecules show the same anisotropy. Thus we have, in each case, a large excess contraction in the out-of-plane direction as indicated by the quadrupole moment $\theta_{NN} = \mu_{NN} - \frac{1}{2}(\mu_{LL} + \mu_{MM})$ which is 0·19 e Å^2 in DFH, 0·16 e Å^2 in FA (edz). In the maps this shows as negative regions below and above the C atom. For the N and O atoms the second-moment differences are severe. The N atom in DFH is slightly contracted in the out-of-plane direction but that in FA shows no such effect. The O atom also seems to contract in DFH and to expand in FA.

The progressively poorer agreement between the two results for higher moments of the density is quite reasonable. In the higher moments the influence of small charges situated far from the atomic nuclei is emphasized. These peripheral portions of the density are weakly bound (in a shallow electrostatic potential) and so highly susceptible to small perturbations, both by chemical substitution in the molecule and by intermolecular interactions in the DFH crystal. Secondly, calculated dipole and quadrupole moments from Hartree–Fock wavefunctions are known to be unreliable. Finally, it is not certain that the atomic partitioning used here is the most appropriate for demonstrating transferability between molecules of very different shape.

Conclusions

Apart from the intrinsic interest in the deformation densities of the two molecules examined, the present study confirms the feasibility of deriving the static deformation density from high-resolution X-ray data. The validity of the deformation refinement on DFH is supported by three tests: (1) The atomic coordinates from this refinement agree with those derived from free-atom refinements on high-order data apart from a small discrepancy in the O atom position; this discrepancy diminishes as the lower cut-off in S for the high-order refinements is increased. (2) The vibration parameters of the C, N and O atoms satisfy the rigid-bond test within their e.s.d.'s and are markedly superior in this respect to the parameters from a high-order refinement. (3) Most convincingly, the deformation density map shows detailed qualitative and semi-quantitative agreement with the SCF deformation density of formamide. The small differences between the two maps must be partly due to inaccuracy in the formamide wavefunction and to failure of transferability between the two molecules and thus provide a rough upper limit to the errors in the experimental deformation density.

These results demonstrate that the difficulties of deconvoluting the vibrational smearing from the observed charge distribution (Coppens & Stevens, 1977) can be satisfactorily surmounted with the aid of an appropriate deformation model provided we have X-ray data of sufficient quantity and quality.

I thank Professors H. Hope and T. Ottersen for making available their low-temperature X-ray data on DFH, and Professor F. L. Hirshfeld for helpful suggestions and advice and for critical reading of the manuscript.

This work was supported by a grant from the United States–Israel Binational Science Foundation (BSF), Jerusalem, Israel.

References

Bingel, W. A. (1963). *Z. Naturforsch. Teil A*, **18**, 1249–1253.

Coppens, P. (1977). *Angew. Chem. Int. Ed. Engl.* **16**, 32–40.

Coppens, P. & Stevens, E. D. (1977). *Isr. J. Chem.* **16**, 175–179.

DENNE, W. A. (1977). *Acta Cryst.* A**33**, 438–440.
DUNNING, T. H. JR (1970). *J. Chem. Phys.* **53**, 2823–2833.
EISENSTEIN, M. (1978). Unpublished.
HAMILTON, W. C. (1965). *Acta Cryst.* **18**, 502–510.
HAREL, M. & HIRSHFELD, F. L. (1975). *Acta Cryst.* B**31**, 162–172.
HASE, H. L., SCHULTE, K. W. & SCHWEIG, A. (1977). *Angew. Chem. Int. Ed. Engl.* **16**, 257–260.
HIRSHFELD, F. L. (1976). *Acta Cryst.* A**32**, 239–244.
HIRSHFELD, F. L. (1977*a*). *Theor. Chim. Acta*, **44**, 129–138.
HIRSHFELD, F. L. (1977*b*). *Isr. J. Chem.* **16**, 226–229.
HOPE, H. & OTTERSEN, T. (1978). *Acta Cryst.* B**34**, 3623–3626.
HOPE, H. & OTTERSEN, T. (1979). *Acta Cryst.* B**35**, 370–372.
HUZINAGA, S. (1965). *J. Chem. Phys.* **42**, 1293–1302.
IRNGARTINGER, H., HASE, H. L., SCHULTE, K. W. & SCHWEIG, A. (1977). *Angew. Chem. Int. Ed. Engl.* **16**, 187–189.
ITOH, K. & SHIMANOUCHI, T. (1972). *J. Mol. Spectrosc.* **42**, 86–99.
KURLAND, R. J. & WILSON, E. B. JR (1957). *J. Chem. Phys.* **27**, 585–590.
METZGAR, T. D. & BLOOR, J. E. (1973). *Quantum Chem. Program Exchange*, **10**, 238.
OTTERSEN, T. (1974). *Acta Chem. Scand. Ser. A*, **28**, 1145–1149.
REES, B. (1977). *Isr. J. Chem.* **16**, 180–186.
REES, B. & MITSCHLER, A. (1976). *J. Am. Chem. Soc.* **98**, 7918–7924.
STENKAMP, L. Z. & DAVIDSON, E. R. (1977). *Theor. Chim. Acta*, **44**, 405–419.
STEVENS, E. D., RYS, J. & COPPENS, P. (1978). *J. Am. Chem. Soc.* **100**, 2324–2328.
SUZUKI, I. (1960). *Bull. Chem. Soc. Jpn*, **33**, 1359–1365.
TELLGREN, R., THOMAS, J. O. & OLOVSSON, I. (1977). *Acta Cryst.* B**33**, 3500–3504.
THOMAS, J. O. (1977). *Acta Cryst.* B**33**, 2867–2876.

Acta Cryst. (1979). B**35**, 2625–2629

Stereochemical Investigations of the Methyl α-D-*threo*- and Ethyl α-D-*erythro* Anomers of 4,6-Di-*O*-acetyl-2,3-dideoxyhex-2-enopyranoside by X-ray Diffraction Methods

BY J. W. KRAJEWSKI, Z. URBAŃCZYK-LIPKOWSKA AND P. GLUZIŃSKI

Institute of Organic Chemistry, Polish Academy of Sciences, 01-224 *Warszawa, Poland*

AND J. BLEIDELIS AND A. KEMME

Institute of Organic Synthesis, Academy of Sciences of the Latvian SSR, Riga, USSR

(*Received* 31 *January* 1979; *accepted* 6 *July* 1979)

Abstract

The stereochemistries of methyl 4,5-di-*O*-acetyl-2,3-dideoxy-α-D-*threo*-hex-2-enopyranoside (THREO) and ethyl 4,6-di-*O*-acetyl-2,3-dideoxy-α-D-*erythro*-hex-2-enopyranoside (ERYTHRO) in the crystalline state have been determined by X-ray diffraction studies. THREO: $C_{11}H_{16}O_6$, $M_r = 244{\cdot}24$, monoclinic, space group $P2_1$ (c unique axis), $Z = 2$, μ(Cu $K\alpha$) = 0·92 mm^{-1}, $d_m = 1{\cdot}29$, $d_c = 1{\cdot}30$ Mg m^{-3}, $a = 5{\cdot}160$ (1), $b = 8{\cdot}971$ (2), $c = 13{\cdot}903$ (2) Å, $\gamma = 103{\cdot}62$ (1)°, $V = 622{\cdot}4$ Å^3. ERYTHRO: $C_{12}H_{18}O_6$, $M_r = 258{\cdot}26$, orthorhombic, space group $P2_12_12_1$, $Z = 4$, μ(Cu $K\alpha$) = 0·872 mm^{-1}, $d_m = 1{\cdot}27$, $d_c = 1{\cdot}29$ Mg m^{-3}, $a = 5{\cdot}377$ (1), $b = 14{\cdot}839$ (2), $c = 16{\cdot}641$ (2) Å, $V = 1327{\cdot}8$ Å^3. The six-membered unsaturated hetero rings appear to have the half-chair $^0H_5$ conformation in both cases. The 2-enopyranosides differ from each other in their 4-*O*-acetyl configurations: pseudo-axial in THREO and pseudo-equatorial in ERYTHRO.

0567-7408/79/112625-05$01.00

Introduction

Recently, Grynkiewicz, Priebe & Zamojski (1979) published a series of syntheses leading to various alkyl 4,6-di-*O*-acetyl-2,3-dideoxy-α-D-*threo*(and -*erythro*)-hex-2-enopyranosides. Two of these, the methyl α-D-*threo*- (THREO, m.p. 332 K) and ethyl α-D-*erythro*- (ERYTHRO, m.p. 352 K) anomers, have been chosen for comparative X-ray diffraction investigations from the point of view of their conformational and geometrical relations.

Experimental

Colourless crystals of THREO and ERYTHRO were obtained by slow evaporation of their solutions in aqueous ethanol. The crystals appear to be unstable in air. Selected crystals were sealed in capillary tubes and used for intensity-collecting procedures. The measurement details and results are presented in Table 1.